



Exploring surface urban heat island (SUHI) intensity and its implications based on urban 3D neighborhood metrics: An investigation of 57 Chinese cities



Yi Zhou ^{a,b}, Haile Zhao ^{a,b}, Sicheng Mao ^{a,b}, Guoliang Zhang ^{a,b}, Yulin Jin ^{a,b}, Yuchao Luo ^{a,b}, Wei Huo ^{a,b}, Zhihua Pan ^c, Pingli An ^{a,b}, Fei Lun ^{a,b,*}

^a College of Land Science and Technology, China Agricultural University, Beijing 100193, China

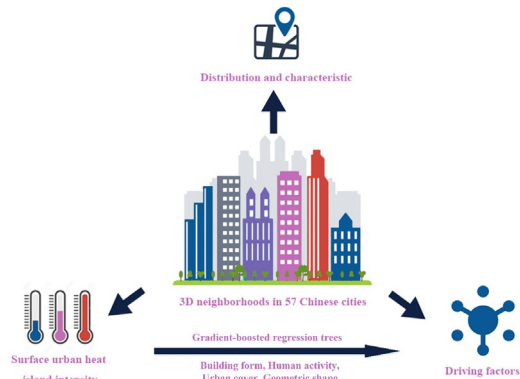
^b Key Laboratory of Land Quality, Ministry of Land and Resources, Beijing 100193, China

^c College of Resources and Environmental Science, China Agricultural University, Beijing 100193, China

HIGHLIGHTS

- 3D neighborhoods and surface urban heat island (SUHI) were mapped in 57 cities.
- High Density & Medium Rise contributed the largest share of the total urban area.
- High Density & Medium Rise and High Density & Low Rise had higher SUHI intensities.
- Urban green and building height played dominant roles in urban heat conditions.
- The industrial and commercial zones in 3D neighborhoods had higher SUHI intensity.

GRAPHICAL ABSTRACT



ARTICLE INFO

Editor: Jay Gan

Keywords:

Urban 3D neighborhood
Surface urban heat island intensity
Gradient-boosted regression trees
Urban form indicator
Chinese cities

ABSTRACT

Excessive urban temperature exerts a substantially negative impact on urban sustainability. Three-dimensional (3D) landscapes have a great impact on urban thermal environments, while their heat conditions and driving factors still remain unclear. This study mapped urban 3D neighborhoods and their associated SUHI (surface urban heat island) intensities in summer daytime across 57 Chinese cities, and then explored their relationships, driving factors as well as implications. Nine categories of urban 3D neighborhoods existed in Chinese cities and the 3D neighborhood of High Density & Medium Rise (HDMR) contributed the largest share of urban areas. The distribution of 3D neighborhoods varied among cities due to their distinct natural and economic traits. The average SUHI intensity can amount to 4.27 °C across all Chinese 3D neighborhoods. High Density & Low Rise (HDLR) and HDMR presented higher SUHI intensities than other 3D neighborhoods in China. Urban green space (UGI) and building height (BH) had great influences on SUHI intensities. The relative contribution of UGI decreased with the increase of building density and building height, but BH presented the opposite trend. The interaction of urban 3D landscapes and function zones led to highly complicated urban thermal environments, with higher SUHI intensities in industrial zones. Besides, the SUHI intensities of 3D neighborhoods presented great diurnal and seasonal variations, with higher SUHI intensities

* Corresponding author at: College of Land Science and Technology, China Agricultural University, Beijing 100193, China.

E-mail addresses: B20193030288@cau.edu.cn (Y. Zhou), SY20203213086@cau.edu.cn (S. Mao), glzhang@cau.edu.cn (G. Zhang), row@cau.edu.cn (Y. Luo), panzhihua@cau.edu.cn (Z. Pan), anpl@cau.edu.cn (P. An), lunfei@cau.edu.cn (F. Lun).

in HDHR and HDMR at nighttime in winter and summer. What's more, urban residents may suffer unequal heat risk inside cities due to the deviations of SUHI intensities among different 3D neighborhoods. It could be a highly effective way to mitigate SUHI effects in cities by increasing urban greening and improving urban ventilation.

1. Introduction

Urban expansion has reshaped local heat fluxes in urban areas, and thus significant temperature differences exist between the urban area and its surrounding rural area, which is defined as the Urban Heat Island (UHI) effect (Kim and Brown, 2021). This UHI effect has brought some urban microclimate problems (Ulpiani, 2021; Liu and Niyogi, 2020), which could be harmful to human health (Amani-Beni et al., 2018; Macintyre et al., 2021; Zander et al., 2018), labor productivity (Matsumoto, 2019) and biodiversity (Peng et al., 2016). At present, about 65 % of global urban residents have suffered the UHI effect, which would have great impacts on local economic development, leading to about 5.6 % of GDP losses by 2100, coupled with future climate change (Estrada et al., 2017). Therefore, urban residential would face more serious heat risks in future, considering continuing urbanization, climate change and population increase; thus, it is of high importance to further focus on UHI effect and explore effective ways to mitigate them in future (Peng et al., 2021).

The heat island is usually known as the Urban Canopy Layer Heat Island (CUHI) and is measured at the standard screen height (1–2 m above ground), below the mean roof height in a thin section of the atmosphere boundary (Stewart and Oke, 2012). The CUHI is mainly estimated with the in-situ observation data (Bechtel et al., 2019), and thus it can hardly illustrate the spatial differences of UHI intensities across large scales, due to limited observation data (Hong et al., 2019). Remote sensing data can be used to retrieval land surface temperature (LST), while the LST differences between urban and rural areas is defined as the Surface Urban Heat Island (SUHI) (Voogt and Oke, 2003). Thus, the remote sensing technology has brought a new viewpoint to understand UHI in large areas, making regional or global studies more efficient and less expensive (Sanyal and Lu, 2004; Zhou et al., 2015b). Due to the advantages of broad detection range and comprehensive space information, the SUHI has been extensively used to investigate urban thermal issues and associated urban heat island effects (Cui et al., 2021; Derdouri et al., 2021; Hu and Brunsell, 2013).

Landscapes exhibit great differences within urban areas, because of their diversity of surface covers, structures, materials, and human activities; thus, significant variations of urban thermal environments also exist inside cities (Geletič et al., 2019; Mirzaei, 2015). Urbanization and urban population demand more high buildings in cities, leading to the urban three-dimension (3D) trait being an important part of urban landscape (Zhang et al., 2019). Previous studies illustrated that urban 3D landscapes (such as building height and building density) could change urban ventilation and thermal conditions, which had great influences on UHI effects (Li et al., 2021; Sun et al., 2020b; Wang et al., 2021a; Zhou et al., 2021). Therefore, it is of high interest to explore how 3D landscapes influence UHI effects (Park et al., 2021). Although some studies have tried to explore the relationships between the UHI intensity and urban 3D landscapes (Li et al., 2021; Sun et al., 2020b; Wang et al., 2021a; Zhou et al., 2021), differences of UHI intensities and their associated driving factors under different 3D landscapes across cities still have received only a few attentions. However, there were still limited knowledge on taking targeted measures to mitigate UHIs. Therefore, it is critical to investigate the UHI intensities and their driving factors under different 3D landscapes, as well as their solutions on mitigating UHI effects.

China has been experiencing rapid urbanization since the reform and opening up in 1978, and >80 % of Chinese cities exhibited increasing UHI intensities (Yang et al., 2019). This rapid urbanization also has greatly changed urban 3D landscapes inside Chinese cities (Guo et al., 2021; Yu, 2021), which could further intensify local UHI effects (Zhang et al.,

2010). Therefore, it is of high importance to better understand the relationship between urban 3D landscapes and their UHI intensities in Chinese cities. Neighborhood, the relative homogenous space within cities, is the basic unit of cities and could also present local urban 3D landscape. Thus, it is beneficial for UHI mitigation and urban planning to explore UHI intensities and their driving factors at the neighborhood scale in China.

To bridge above gaps, we aimed to map urban 3D neighborhoods as well as their SUHI intensities across 57 Chinese cities, based on building height and building density; then, we explored the relationships between 3D neighborhoods and their SUHI intensities. In detail, our study aimed to: (1) identify and map urban 3D neighborhoods varied across 57 Chinese cities; (2) explore their SUHI intensities across different urban 3D neighborhoods in the summer daytime of 2017–2019; (3) reveal how different urban form indicators influence SUHI intensities across different urban 3D neighborhoods; (4) finally discuss how to mitigate SUHI effects at the urban 3D neighborhood scale.

2. Methodology

2.1. Study area

A total of 57 Chinese cities were selected to identify their 3D neighborhoods as well as their SUHI intensities in this study, including four municipalities (Beijing, Shanghai, Tianjin and Chongqing), 15 sub-provincial cities and 37 prefectural-level cities (Fig. 1). Except the northern temperate zone (<2 % of the total area in China), these 57 cities covered all the remaining climatic zones in China, and thus they can provide comprehensive information for UHI in China. What's more, these cities played an important role in local economic development, and they together contributed to 37 % of Chinese total GDP in 2020. Besides, their urban built area has been increasing and totally covered 93,264 km² in 2020, about 8 times larger than that in 1990 (National Bureau of Statistics of China, 2021). Higher buildings, less green space and more crowded districts also occur in these cities, and thus their 3D landscapes have been changing in last decades. Due to urban expansion, population increase and 3D landscape change, their land surface temperature during summer daytime has increased by about 9 °C in Chinese cities during last 20 years (Wan et al., 2021).

2.2. Research framework and data source

Fig. 2 presented our research framework, and it included four main steps: (1) Identifying each neighborhood in these cities: Based on the information of road networks from the OpenStreetMap (<https://wordpress.org/plugins/osm>), each neighborhood with buildings was identified in this study. (2) Mapping 3D neighborhoods: The Baidu Map (one of the biggest free map suppliers in China, <https://lbsyun.baidu.com/>), presented detailed building information, including their location, shape, height and so on. We obtained all the building information from the Baidu Map, and then estimated the average value of building density and building height for each neighborhood. Thus, according to all above information, 3D neighborhoods were mapped in these 57 cities. (3) Mapping SUHI intensities for each 3D neighborhood: With the split-window algorithm method, Google earth engine (GEE) and Landsat 8 OLI were used to estimate the average LST of summer daytime across June to September in 2017–2019. According to the LST differences between each neighborhood and its surrounding rural areas, we mapped SUHI intensities of different 3D neighborhoods in these 57 cities; (4) Exploring relationships between urban form indicators and their SUHI intensities for different 3D neighborhoods. In this study,

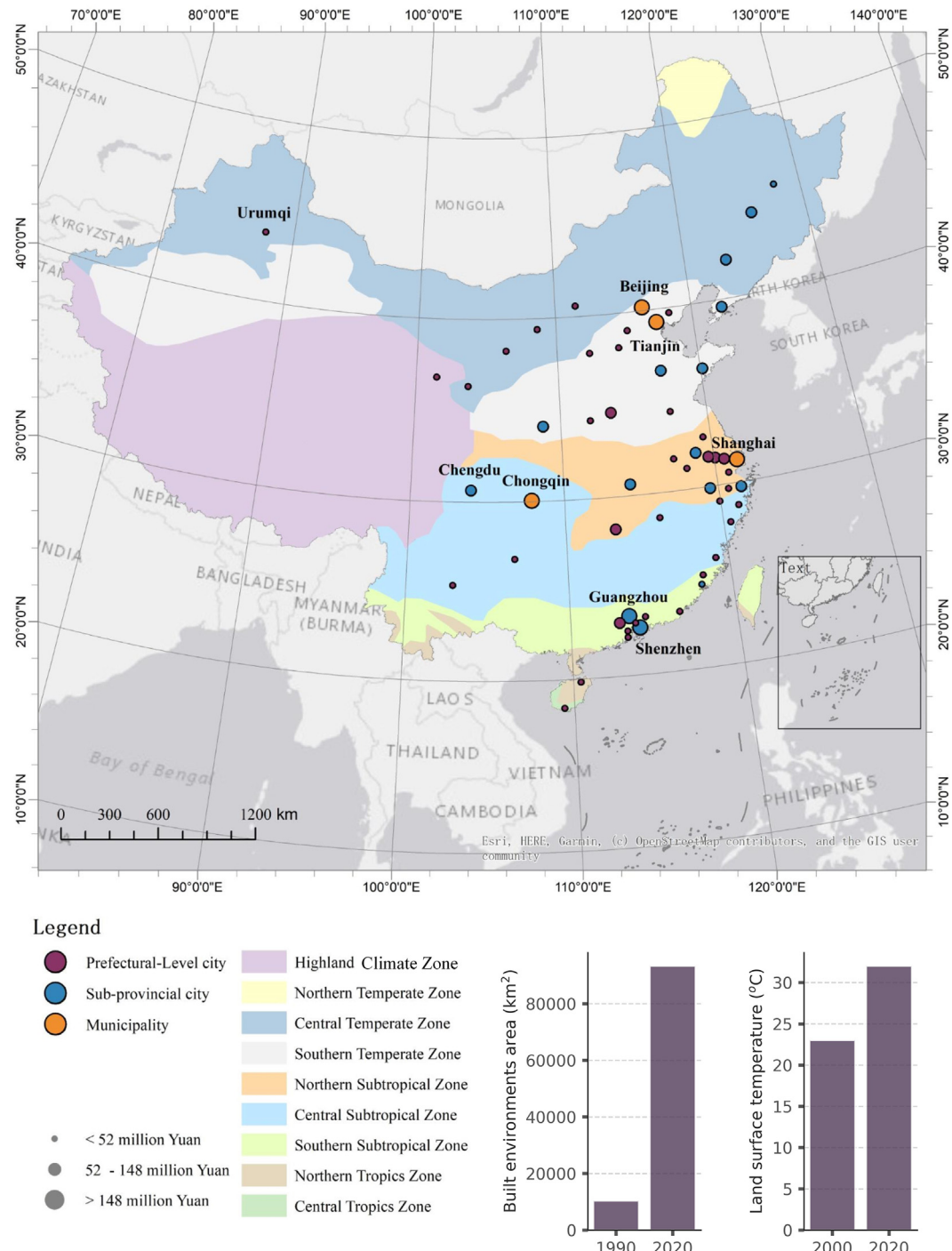


Fig. 1. Our study area and its associated social-economic levels.

we explored relationships between urban form indicators and their SUHI intensities for different 3D neighborhoods (more detailed information see the following Table 1 and the following section). More energy consumption due to large population has increased anthropogenic heat emission in cities, but it can hardly be diffused with intensive compact buildings and impervious surfaces, resulting in serious urban thermal problems there (Liang et al., 2020); conversely, the blue space (like water) and the green space (like forest and grass) presented significant cooling effects in cities (Aram et al., 2019; Hamada and Ohta, 2010). Besides, the geometry of neighborhood also has some influences on SUHI (Li et al., 2021; Sun et al., 2020a; Wang et al., 2021a; Zhou et al., 2021). Therefore, we selected 10 urban form indicators in this study to explore their relationships with urban 3D

neighborhood SUHI intensities, including (1) five building form indicators of building height (BH), the standard deviation of building height (STDBH), building surface fraction (BSF), sky view factor (SVF), and frontal area index (FAI); (2) three urban cover indicators of urban impervious surface area (UISA), Urban Green Index (UGI) with the average normalized difference vegetation index (NDVI) and Urban Blue Index (UBI) with the average normalized difference water index (NDWI); (3) one geometric shape indicator of compactness of neighborhood (CI). Besides, although “human activity” is not a measure of urban form, it is correlated to urban form. Therefore, we also selected one human activity indicator of the population (POP) to study its relationship with SUHI. More detailed calculation methods were shown in Table 2.

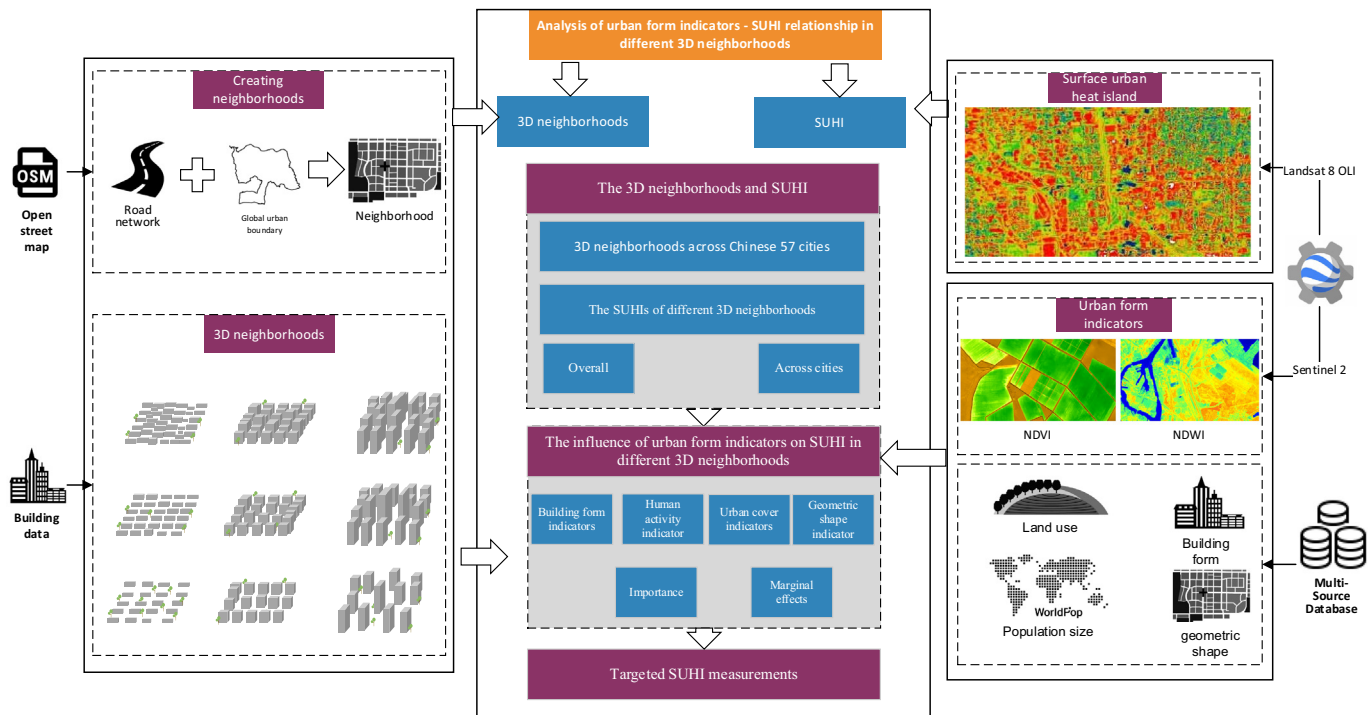


Fig. 2. The framework of our research.

2.3. Mapping 3D neighborhoods

To map 3D neighborhoods, we fixed geometry errors of the OSM road network and extended all roads by 100 m to reduce the number of disconnected roads. Based on this, we converted them into polygons and excluded polygons with a total area $< 1000 \text{ m}^2$ and $> 10 \text{ km}^2$ to avoid fragmented or huge neighborhoods. We defined our neighborhood as polygons with buildings and then calculated the average building height (BH) and building density (BSF) of each neighborhood. Considering their traits in China, building height and building density can be divided into three different levels, respectively: Low rise (1–3 floors), Medium rise (4–7 floors) and High rise (8 floors and above) for building height, and Low density (0–0.15), Medium density (0.15–0.25) and High density (0.25 and above) for building intensity. Therefore, it can be used to investigate 3D urban form and also to study their associated UHI, coupling building density and building height (Long et al., 2019; Sun et al., 2020a). Based on these two facets, all urban neighborhoods can be divided into 9 categories of urban 3D neighborhoods in China as follows (Fig. 3): High Density & Low Rise (HDLR), High Density & Medium Rise (HDMR), High Density & High Rise (HDHR), Medium Density & Low Rise (MDLR), Medium Density & Medium Rise (MDMR), Medium Density & High Rise (MDHR), Low Density & Low Rise (LDLR), Low Density & Medium Rise (LDMR), and Low Density & High Rise (LDHR).

2.4. Surface urban heat island (SUHI) intensity of urban 3D neighborhoods

2.4.1. Land surface temperature

Without any atmospheric profile information, the split-window algorithm has widely been used to monitor sea or land surface temperature (Merchant et al., 2008; Wan and Dozier, 1996). Here, the normalized difference vegetation index (NDVI) method was used to derive land surface emissivity values (Li and Jiang, 2018). To retrieve the emissivity corrected LST values from the Landsat data, the preprocessed thermal bands produced by radiometric calibration and atmospheric correction using Google Earth Engine, were used as follows:

$$LST = \frac{T_B}{1 + \left(\alpha \times \frac{T_B}{\beta} \right) \times \ln(\varepsilon)} \quad (1)$$

where T_B = at-satellite brightness temperature in degrees Kelvin; α = wavelength of emitted radiance ($\alpha = 10.8 \mu\text{m}$ for Landsat-8 OLI/TIRS band 10); $\beta = h \times \frac{c}{\sigma(1.438 \times 10^{-2} \text{ m K})}$; σ = Boltzmann constant ($1.38 \times 10^{-23} \text{ J K}^{-1}$), h = Planck's constant ($6.626 \times 10^{-34} \text{ J s}$), and c = velocity of light ($2.998 \times 10^8 \text{ m/s}$); and ε is the land surface emissivity estimated using the NDVI method. The resulting LST values were later converted from degrees Kelvin to degrees Celsius ($^{\circ}\text{C}$).

Table 1

Data source in our research.

Data	Time	Resolution	Usage	Source
Landsat 8 OLI	June to September 2017–2019	30 m	Estimating SUHI intensities	https://search.earthdata.nasa.gov/search
Sentinel-2	June to September 2019	10 m	Estimating NDVI and NDWI	
OSM road network	2020	Vector data	Identifying neighborhoods	https://wordpress.org/plugins/osm/
Global urban boundary 2018	2018	Vector data		http://data.ess.tsinghua.edu.cn/
FROMGLC-10	2017	10 m	Extracting urban impervious surface	
Population	2019	100 m	Estimating the population of neighborhoods	http://www.worldpop.org
Building data	2019	Vector data	Estimating building forms of neighborhoods	https://lbsyun.baidu.com/
Meteorological data	2019	Statistical data	Determine the wind direction.	https://data.cma.cn/

(Note that the building data source (<https://lbsyun.baidu.com/>) is in Chinese).

Table 2

Main urban form indicators in our research.

Urban form indicators	Formula	Definition	Data source
BH (Building Height)	$BH = \frac{\sum_{i=1}^n BS_i * BH_i}{\sum_{i=1}^n BS_i}$	n is the number of buildings in each neighborhood. BS_i is the floor area of a building. BH_i is the floor number of the building.	This indicator was calculated from building data, unit is meter (Zhou et al., 2021).
STDBH (Standard Deviation of Building Height)	$STDBH = \sqrt{\frac{1}{n} \sum_{i=1}^n (BH_i - BH_m)^2}$	n is the number of buildings in each neighborhood. BH_i is the building height of a building. BH_m is the average building height in the neighborhood.	This indicator was calculated from building data; unit is meter (Zhou et al., 2021).
BSF (Building Surface Fraction)	$BSF = \frac{\sum_{i=1}^n BS_i}{S}$	S is the area of each neighborhood.	This indicator was calculated from building data (Zhou et al., 2021)
SVF (Sky View Factor)	$SVF_i = \frac{SS_{sky}}{SS_{sky} + \sum S_b}$ $SVF = \frac{\sum_{i=1}^n SVF_i}{n}$	SVF_i is the SVF value of a point in the non-building area ($1 m \times 1 m$). n is the number of SVF points ($30 m \times 30 m$) in the non-building area. S_{sky} and ΣS_b is the area of the sky and the area occupied by the building at a particular point. $S_{sky} + \Sigma S_b$ is the entire hemisphere environment at a certain point.	This indicator was calculated from building data (Zhou et al., 2021).
FAI (Frontal Area Index)	$FAI_{(0)} = \frac{A_{P0} Z_{meanT}}{A_T}$ $FAI = \sum_{\theta=1}^N \lambda_{f(\theta)} B_\theta$	$\lambda_{f(\theta)}$ is the FAI, A_{P0} is the projected area under wind direction θ , A_T is the horizontal base area, Z_{meanT} is the average height of the bottom grid, B_θ is the wind frequency in wind direction θ , and λ_f represents the weighted average of $\lambda_{f(\theta)}$ that is independent of the wind direction. Herein, wind direction data with 16 cardinal directions were selected to represent the wind-frequency weighted arithmetic mean.	This indicator was calculated from building data and wind direction data (Mao et al., 2022).
POP (Population)	$POP = \sum_{i=1}^n POP_i$	n is the number of pixels in neighborhood, POP_i is the population size of the neighborhood at each pixel.	This indicator was collected from the open spatial demographic dataset of WorldPop
UISA (Urban Impervious Surface Area)	$UISA = \frac{S_u}{S}$	S_u is the total area of the urban impervious surface in the neighborhood.	This indicator was calculated from the FROMLC-10 dataset (Chen et al., 2019).
UGI (Urban Green Index)	$UGI = \frac{\sum NDVI_i}{n}$	N is the number of pixels in neighborhood, $NDVI_i$ is the NDVI value at each pixel in summer.	It was calculated from Sentinel – 2 using GEE.
UBI (Urban Blue Index)	$UBI = \frac{\sum NDWI_i}{n}$	N is the number of pixels in neighborhood, $NDWI_i$ is the NDWI value at each pixel in summer.	It was calculated from Sentinel – 2 using GEE.
CI (Compactness Index)	$CI = \frac{sqr(A)}{E}$	E is the perimeter of the neighborhood. A is the area of the neighborhood.	It was calculated from the neighborhood data

2.4.2. Estimation of surface urban heat islands

The SUHI intensity was calculated as the difference of the average LST in summer daytime between the urban area and its corresponding rural area (about the 20 km buffer zone of the urban boundary). To reduce the impacts of topography and land use, we reserved only green spaces (like grassland, cropland and forest land) in rural areas with topographic relief of fewer than 5 m (the minimum rural area was 900 m², because the LST spatial resolution was 30 m). Therefore, the SUHI intensity can be estimated as follows:

$$SUHI_{ij} = ULST_{ij} - ELST_i \quad (2)$$

where $SUHI_{ij}$ is the SUHI intensities of city i at neighborhood j , $ULST_{ij}$ is the LST of city i at neighborhood j , $ELST_i$ is the LST of the corresponding ex-urban references in city i .

2.5. The relationship between urban form indicators and SUHI intensity

The Gradient-boosted regression trees (GBRT) method is selected to illustrate the relationship between urban form indicators and SUHI intensity, with its principle of multivariate systems (Kedem et al., 2012). The GBRT method can provide important scores for each feature, and thus it can be used to quantify the relative contributions of different variables. Moreover, the GBRT method can also produce a partial dependence relationship to explain the marginal effect of each predictor variable on the response variable (Heilmayer and Brey, 2003). Therefore, it can be used to disentangle the relationship between LST and environmental variables (Logan et al., 2020). In our study, the GBRT model is developed by python (Pedregosa et al., 2011) to study the relationship between urban form indicators and SUHI intensity. For training and validation, the SUHI intensities and urban form indicators of 113,671 neighborhoods in China are separated into testing (80 %) and validation groups (20 %). Based on this, the feature

importance of each urban form indicator is calculated to investigate their relative contributions to SUHI intensities, and the two-dimensional partial dependence plot is drawn to investigate the interactions on SUHI intensities between the two urban form indicators which contribute the most to SUHI intensities. However, the spatial resolution of these raster datasets varied, such as population map and urban green index, and we have resampled these raster data into 30 m, because the spatial resolution of LST was 30 m.

3. Results

3.1. The urban 3D neighborhoods across 57 Chinese cities

There was a total of 113,671 urban neighborhoods in these 57 Chinese cities, 60 % of which were located in municipalities and prefectural-level cities; what's more, megacities presented more urban neighborhoods there, especially in Beijing (12,043 urban neighborhoods) and Shanghai (8769 urban neighborhoods) (Fig. 4a). Besides, most neighborhoods presented <10 floors of building height and 0.5 of building density in China, with their average of 5 floors and 0.29 (see SI). Therefore, the urban 3D neighborhood of High Density & Medium Rise (HDMR) contributed the largest share in Chinese cities (36 %) (Fig. 4a), followed by the High Density & Low Rise (HDLR, 16 %) and Medium Density & Medium Rise (MDMR, 12 %). However, since Chinese cities were usually crowded, the neighborhood of Low Density & High Rise (LDHR) contributed the least share of 4 %. More developed cities or mountainous cities significantly presented higher building height than other cities, with a positive value of $p < 0.01$; however, high density neighborhoods existed in all cities (Fig. 4c). Therefore, the proportion of 3D neighborhoods presented great variations among all these 57 cities in China. As shown in Fig. 4a, the neighborhoods with medium rise contributed the largest share of 76 % in Yinchuan, while high density neighborhoods could amount to 82 % in Shantou. Due to the large urban area and relatively less population, only a

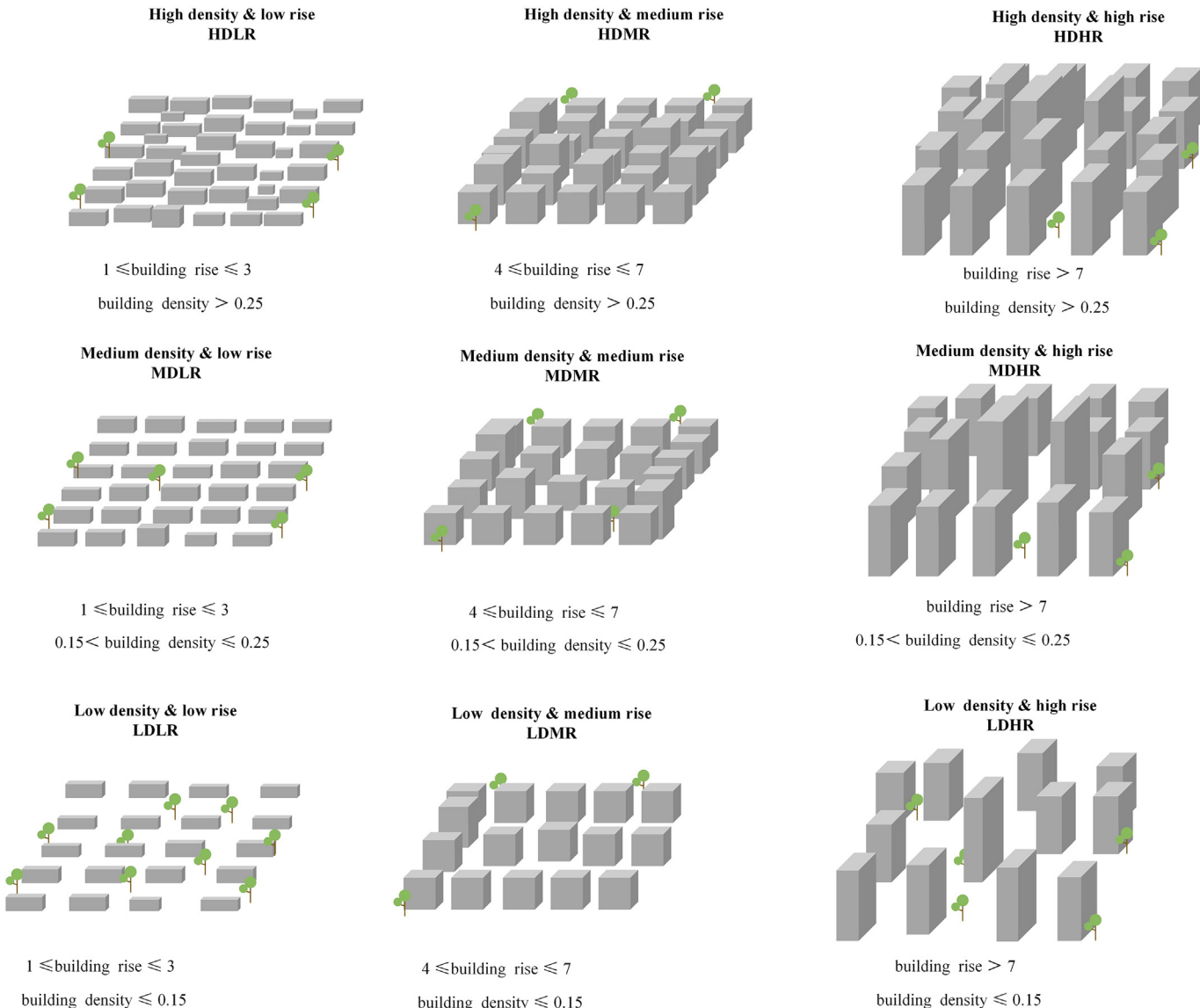


Fig. 3. The nine categories of urban 3D neighborhoods in China.

few high-rise buildings existed in some small or medium cities (like Luoyang and Shantou), and thus the neighborhoods of LDHR and MDHR presented a limited proportion there (totaling to 6.9 % there). With less flat area, the average building height in mountainous cities was much higher than other cities, and hence their 3D neighborhood of HDHR presented a higher proportion there (up to 20 % in Chongqing). Traditional culture would also have a great influence on urban 3D neighborhoods, especially traditional buildings. Although being a developed and crowded megacity, Beijing still had a large share of HDLR neighborhoods, and it was because the famous and traditional building of Hutong was widely located in Beijing.

3.2. The SUHI intensities of different 3D neighborhoods among cities

The SUHI intensity of urban 3D neighborhoods mainly ranged from 2 °C to 6 °C in these 57 Chinese cities, with the average SUHI intensity of 4.27 °C (Fig. 5b). In particular, eastern and southern Chinese cities presented higher SUHI intensities than cities in other regions, due to higher temperature and better socio-economic levels. Notably, the abundance of urban green space could lead to lower temperature than its nearby area of desert, and thus Urumqi in Northwest China presented the urban cold island effect of -0.27 °C (Fig. 5a). Urban 3D landscape had a clear impact on SUHI intensity across 57 Chinese cities, with a difference of P value <0.05 among

3D neighborhoods (Fig. 5c). In compact neighborhoods with higher population densities, huge anthropogenic heat was emitted but hardly be diffused outside or absorbed by green space, and thus these 3D neighborhoods presented higher SUHI intensities. Consequently, the highest average SUHI intensity of 5.3 °C was distributed in the 3D neighborhood of HDLR, followed by HDMR (4.6 °C). Besides, the SUHI intensities in HDLR and HDMR were also higher than other 3D neighborhoods in all cities, particularly in Wenzhou with the SUHI intensity of HDLR > 8 °C (see SI). However, for 3D neighborhoods with medium or high building density, their SUHI intensities decreased with building height, because the shade of tall buildings could play the cooling effect there and thus their LST presented relatively lower than surrounding neighborhoods. Therefore, the 3D neighborhood of MDHR had the lowest SUHI intensity of 2.9 °C, followed by LDHR (3.1 °C). Great differences of SUHI intensities existed among different climate zones, but HDLR and HDMR still presented higher SUHI intensities than other 3D neighborhoods in all climate zones (Fig. 5d), which should gain more attentions in future.

3.3. Urban form indicators and SUHI intensities for 3D neighborhoods

Urban green index (UGI) had the largest impact on SUHI intensities (62 %), followed by BH (27 %); thus, these two urban form indicators

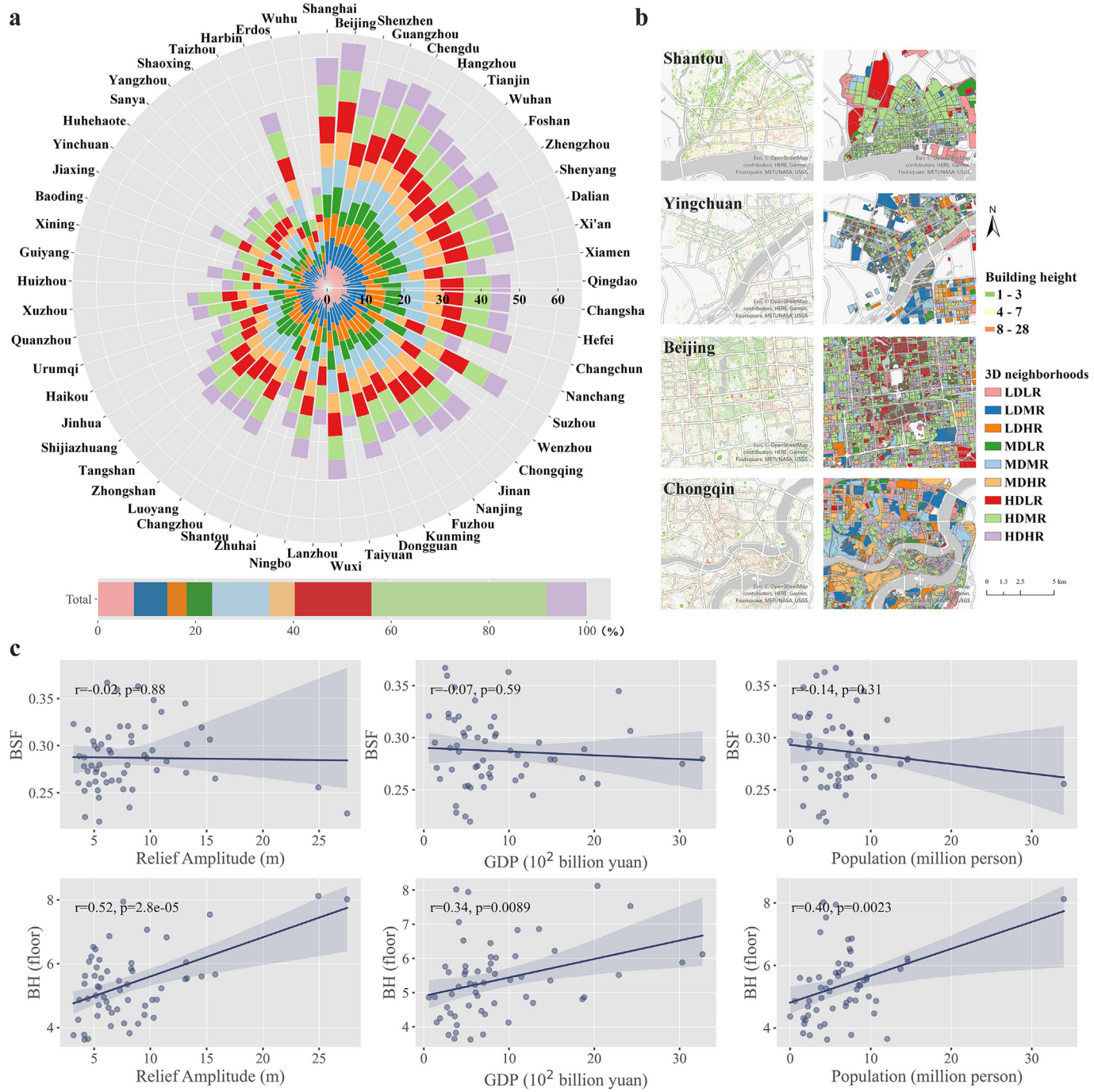


Fig. 4. The 3D neighborhoods in all 57 cities (a, the numbers and percentage of 3D neighborhoods among 57 cities, note that the numbers of 3D neighborhoods were logged; b, typical 3D neighborhoods in some cities; c, the relationship between BSF (BH) and other factors).

together played the dominant role in the SUHI effect across Chinese cities (Fig. 6). Both UGI and BH had negative relationships with SUHI intensities, with higher SUHI intensities in lower building or lower urban green areas (Fig. 6a). Besides, urban form indicators of UBI, STDBH and FAI also presented negative relationships with SUHI intensities. For all 3D neighborhoods, the two dominant indicators of UGI and BH can lead to a total impact of 2.73 °C on the SUHI intensity, but it varied between 1.68 and 3.56 °C among different urban 3D neighborhoods. Moreover, the total SUHI intensity decreased with the increase of building density and building height. Besides, their SUHI intensities were almost independent with BH in 3D neighborhoods with $UGI > 0.15$, while a stronger dependence between BH and SUHI intensity presented in 3D neighborhoods with $UGI < 0.1$.

Except the 3D neighborhoods of HDHR, UGI still had the largest impact on SUHI intensity for all the remaining 3D neighborhoods, but its contribution decreased with the increase of building height and building density. Conversely, the contribution of BH increased with the increase of building height and building density, and its relative contribution can amount to 34 % in the 3D neighborhood of HDHR. However, the relative contribution of BH was smaller than STDBH, FAI and UBI in most neighborhoods with low or medium building rise. Besides, CI had the smallest relative contribution to SUHI intensity (3 %) in all 3D neighborhoods, and thus only optimizing neighborhood geometric shape could have limited effects on mitigating SUHI effects in Chinese cities.

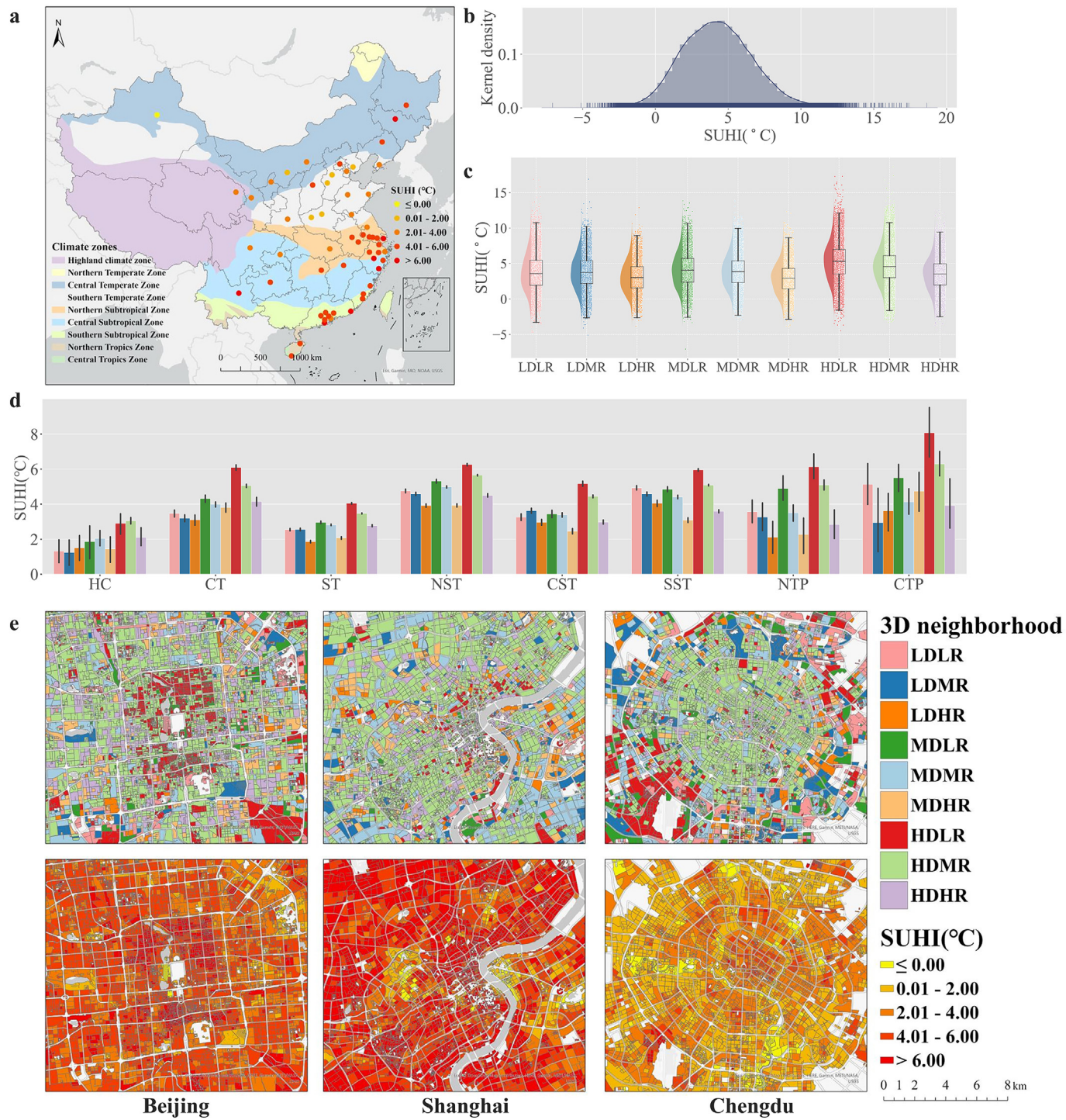


Fig. 5. The urban 3D neighborhoods and their SUHIs in different cities during summer daytime (a: the average SUHI intensities of Chinese cities. b: the distribution of SUHI intensities in each city. c: the average SUHI intensities of 3D neighborhoods. d: the average SUHI intensities of 3D neighborhoods in different climate zones, note: HC is Highland Climate Zone; CT is Central Temperate Zone; ST is Southern Temperate Zone; NST is Northern Subtropical Zone; CST is Central Subtropical Zone; SST is Southern Subtropical Zone; NTP is Northern Tropics Zone; CTP is Central Tropics Zone. e: the average SUHI intensities of 3D neighborhoods in typical cities.)

4. Discussion

4.1. Results compared with other studies

The simple division of rural area and urban area could lead to uncertainties of SUHI intensities, due to their differences of rural area in different cities (Cao et al., 2017; Martin-Vide et al., 2015; Varquez and Kanda, 2018). As a result, we contrasted the SUHI intensities of each neighborhood in our

research with the SUHI intensities from MODIS LST data (Chakraborty and Lee, 2019). The results showed that there was a positive relationship among them ($r = 0.46, p < 0.01$) (Fig. 7a), and the MODIS SUHI intensities of different 3D neighborhoods also presented a similar trend (Fig. 7b). Although the diversities of data source and estimation method could lead to some differences of SUHI among different studies, our SHUI results can be used to explore their thermal conditions among different 3D neighborhoods. Besides, remote sensing technology was widely used for mapping 3D urban

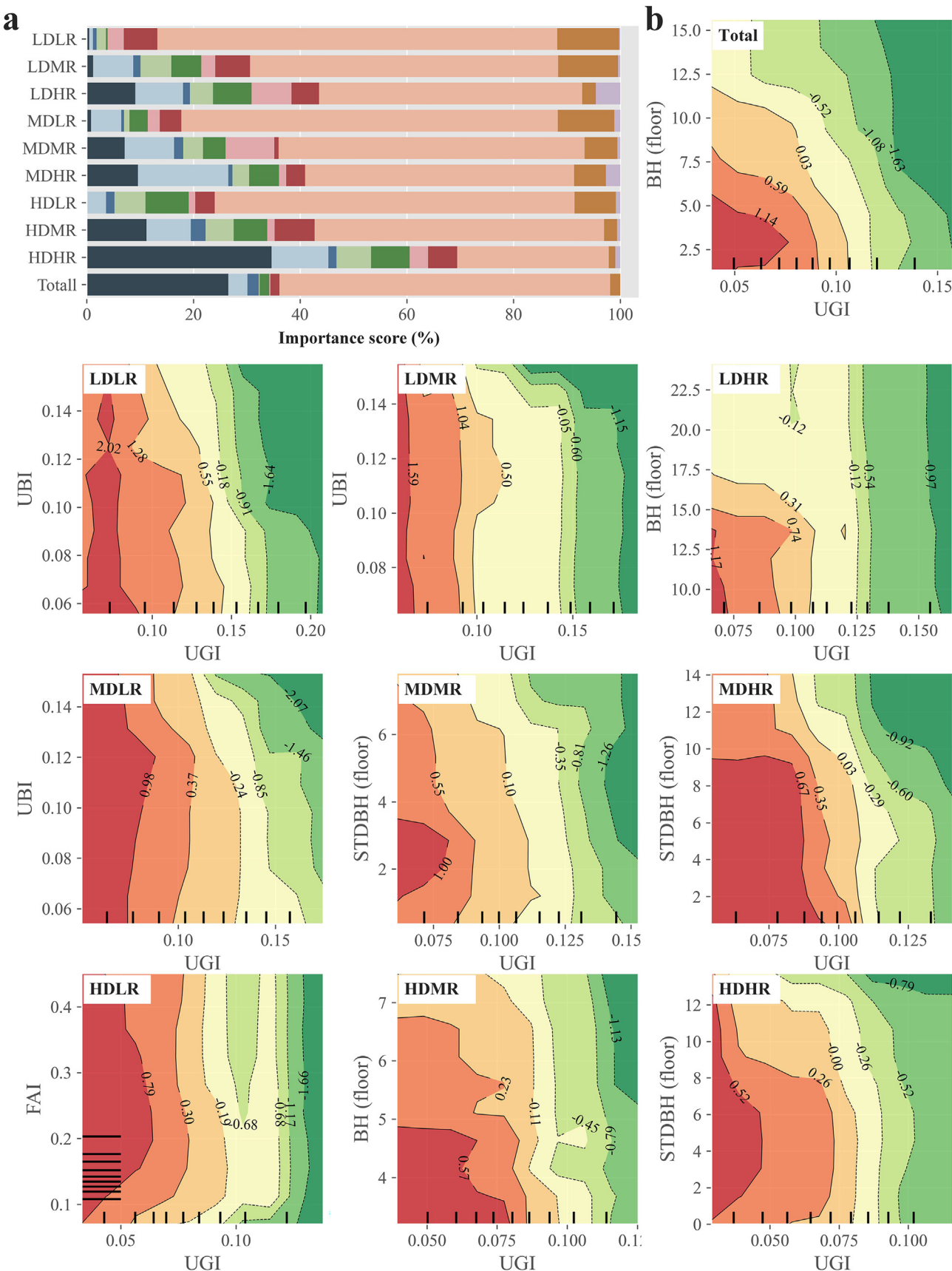


Fig. 6. The relationship between urban form indicators and SUHI intensities (a: the two-dimensional dependence plots of two dominant urban form indicators to SUHI intensities. b: the contribution of different urban form indicators to SUHI intensities.)

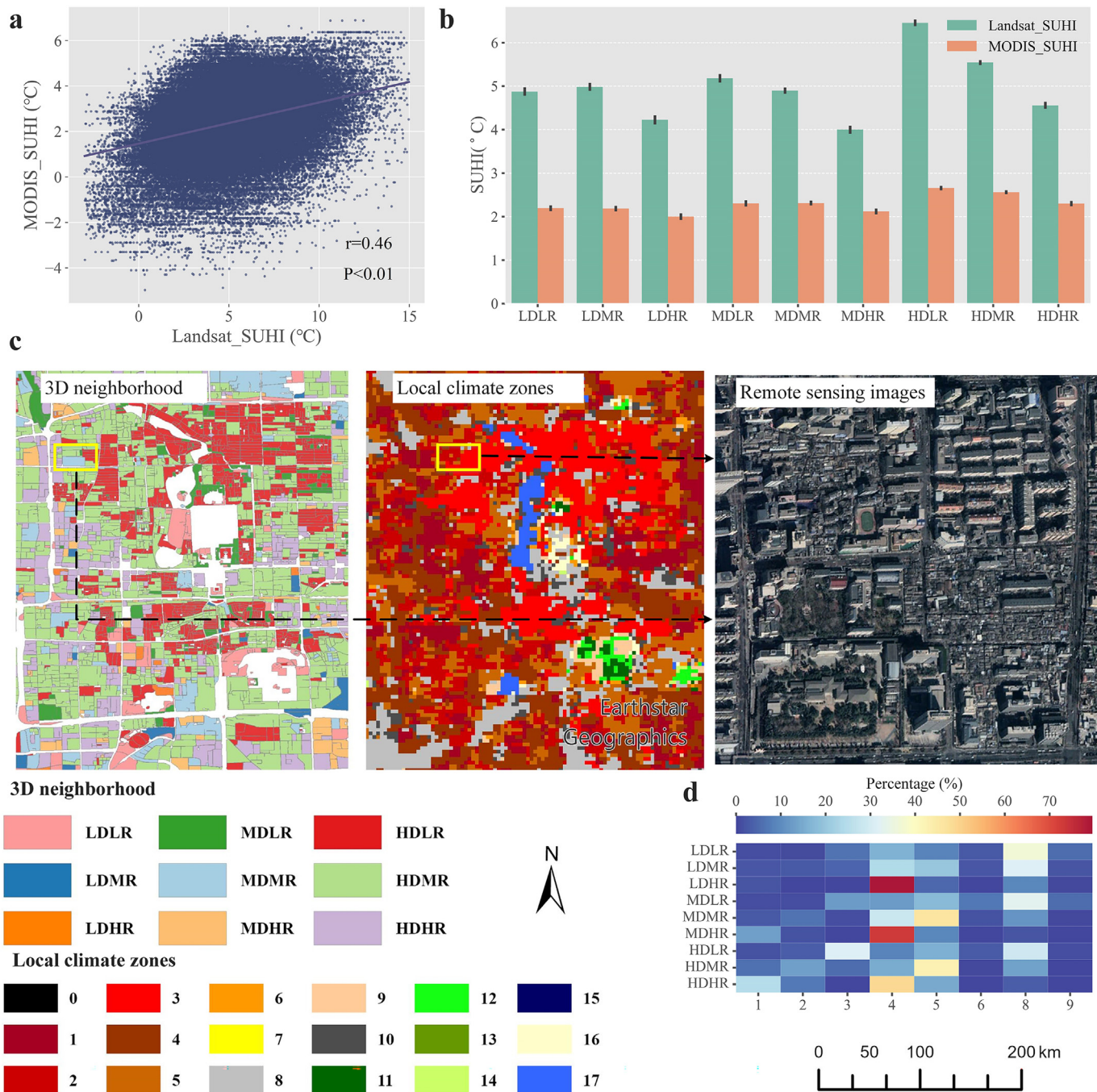


Fig. 7. The comparison of our results with other studies (a: the SUHI relationship between our results and other study. b: the average SUHI intensities of 3D neighborhoods in our results and other study. c: the spatial distribution of building data, 3D neighborhoods and local climate zones in Beijing. d: the percentages of 3D neighborhoods fall into different local climate zones. Note that: 1 is compact high-rise, 2 is compact midrise, 3 is compact low-rise, 4 is open high-rise, 5 is open midrise, 6 is open low-rise, 7 is lightweight low-rise, 8 is large low-rise, 9 is sparsely built, 10 is heavy industry, 11 is dense tree, 12 is scatter tree, 13 is bush and scrub, 14 is low plants, 15 is bare rock or paved, 16 is bare soil or sand, 17 is water, 0 is no data).

landscapes at the large scale (Li et al., 2020; Qi et al., 2016), and thus Zhu et al. (2022) mapped global local climate zones (LCZ) using Sentinel-1 and Sentinel-2. Thus, we generated 500 random points in Beijing to compare our results with Zhu's results. Both our 3D neighborhood and local climate zone can present spatial differences of urban 3D landscapes inside cities (Fig. 7c), and the neighborhood of LDHR presented the maximum similarity with the LCZ of open high-rise ($> 70\%$) (Fig. 7d). However, great differences of classification methods existed between 3D neighborhood and LCZ, and thus most 3D neighborhoods presented limited similarities with this global LCZ product (Fig. 7d). More importantly, as shown in Figs. 7c,

3D neighborhoods derived from building data could provide more detailed information of building information at the neighborhood scale, which could better present urban 3D landscapes at the small scale.

4.2. The SUHI intensities of 3D neighborhoods in nighttime and different seasons

SUHI intensities varied greatly across time and season, due to changes of solar radiation and weather conditions (Du et al., 2016; Sun et al., 2020c; Zhang et al., 2017). Therefore, it is important to investigate the SUHI intensities of 3D neighborhoods at nighttime as well as different

seasons. However, due to the limited data of Landsat 8 OLI at nighttime across these 57 cities (considering weather conditions and transit time), we only estimated the SUHI intensities using Landsat 8 OLI in winter daytime. Meanwhile, the nighttime SUHI intensities were collected from Chakraborty and Lee. (2019). The results showed that all cities had the “heat island” effect at nighttime, but some of them presented the “cold island” effect in winter daytime, especially for some northern cities (like Shenyang and Taiyuan) (Fig. 8a). The similar observation during winter daytime was also found in other studies, and it was mainly related to local serious air pollution (Zhou et al., 2015a). A large amount of coal was burned for heating in winter due to their cold weather, and thus heavy air pollution often occurred in these northern cities. Compared to

its nearby rural area, heavy air pollution with PM2.5 could hamper the short wave of solar radiation arriving the urban land surface in urban areas, and lower surface land temperature would occur there (He et al., 2002; Sang et al., 2000). Besides, the SUHI intensities among 3D neighborhoods also presented great variations at different times. With more higher buildings and intensive building density, the majority of heat can hardly disperse outside from these neighborhoods and mainly be blocked here at nighttime; thus, the neighborhoods HDHR and HDMR presented higher SUHI intensities than other neighborhoods. Consistent with the summer daytime, the neighborhood of HDLR also had the highest SUHI intensities in winter daytime, because of more direct sunlight but poor ventilation here (Fig. 8).

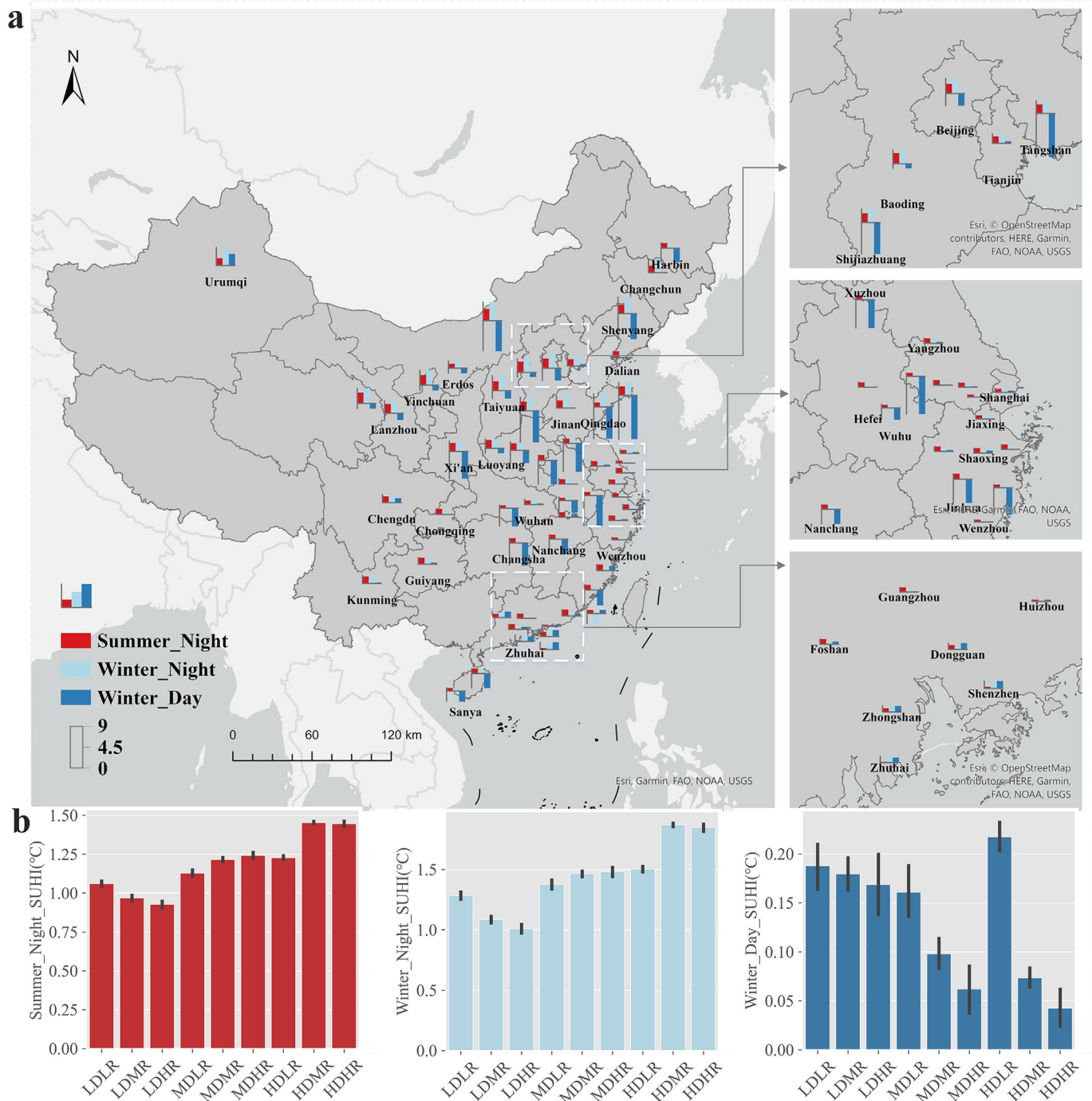


Fig. 8. The SUHI intensities of 3D neighborhoods at nighttime and during different seasons (a: the SUHI intensities at nighttime and during different seasons among each city. b: the SUHI intensities of 3D neighborhoods at nighttime and during different seasons.)

4.3. Urban function zones complicated the heat conditions of 3D neighborhoods

The city was a highly-populated area with various socioeconomic activities, and thus it could be divided into different function zones, like industrial zone and commercial zone (Yu et al., 2021). Different function zones presented different population densities and socio-economic activities, and thus they could also present significant differences of urban 3D landscapes and SUHI intensities (Changnon, 1992; Peng et al., 2012; Yao et al., 2019). Besides, limited urban areas led to more multifunctional zones, which were also attributed to complex 3D landscapes (Motieyan and Azmoodeh, 2021). Therefore, there was a need to explore the 3D landscapes and SUHI intensities among different urban function zones. According to 10-m satellite images, OpenStreetMap, nighttime lights, POI and Tencent social big data, Gong et al. (2020) mapped urban land use across China. With the help of this dataset, all neighborhoods were divided into five function zones in our study, including the residential zone, industrial zone, commercial zone, public service zone, and transportation zone. While HDMR was still the most common neighborhood in different function zones, there were significant differences of urban 3D landscapes among different function zones. The commercial zone was usually as a space for economic activities in urban areas (Wu et al., 2018), like the central business district (CBD). Therefore, the commercial zone usually located in the central or populated areas that were expensive (Garang et al., 2021). However, these areas were limited within cities, thus, the commercial zone was usually occupied by a larger proportion of the HDLR neighborhoods. Besides, in order to handle more vehicles or stations without congestion, the transportation zone was mainly concentrated by the 3D neighborhood of LDLR (Fig. 9). More importantly, there also were great differences in SUHI intensities among these function zones (see SI). In particular, the industrial zone had the highest SUHI intensities for these same 3D neighborhoods (Huang and Wang, 2019), and it was because more factories in this zone could consume a great deal of energy and thus release a large amount of heat (Li et al., 2014). Therefore, it was indicated that urban thermal environment was influenced not only by urban 3D neighborhoods but also by socio-economic activities. Therefore, urban 3D neighborhood and their associated economic function made the urban thermal environment more complicated. Hence, it is of high importance to explore how to mitigate urban SUHI intensities, considering their 3D landscape and function zones.

4.4. Implications and shortcomings

We mapped 3D neighborhoods in 57 Chinese cities and investigated their distribution and SUHI intensities, allowing us to gain a better understanding of the 3D landscapes and the most "heat vulnerable" 3D neighborhood in Chinese cities. Therefore, it is beneficial for the reduction of

potential thermal inequalities within urban areas. More importantly, different from previous studies (Sun et al., 2020a; Zhang et al., 2019), we mainly studied the SUHI intensities and their driving factors across different 3D neighborhoods, which may be useful to mitigate urban thermal issues with targeted measures. Generally, due to different urban 3D landscapes, urban residents suffered unequal SUHI intensities inside cities (Buyantuyev and Wu, 2010). Local poor and marginal residents could not afford higher housing prices, and thus they usually lived in old and compact neighborhoods (like HDLR), which could suffer more serious SUHI effects (Mashhoodi, 2021). According to present studies, the poor in the United States, South Africa and Brazil had suffered more burdens of SUHI effects (Chakraborty et al., 2019; Chen et al., 2021). Zhou et al. (2021) also pointed out that residents in Hutong, the typical 3D neighborhood of HDLR in Beijing, suffered more serious heat risks than other local climate zones. The unequal heat risk could be a great issue in future, considering future climate change and urbanization, and thus it is of high importance to make some adaptation measures for these vulnerable residents (Cheng et al., 2021; Fleming et al., 2018). Researchers have already focused on mitigating the SUHI effect by many methods, such as improving urban ventilation, optimizing local climate zones and urban landscapes (He et al., 2020; Leconte et al., 2015). According to our study, increasing green spaces in cities could be one of the highly effective ways to mitigate SUHI inside cities (Aram et al., 2019; Hamada and Ohta, 2010). Therefore, there were some cooling strategies for increasing green spaces in cities, including building pocket parks in neighborhoods with low or medium building density or replacing traditional roofs with green roofs in compact neighborhoods (Kumar and Kaushik, 2005; Lin et al., 2017). Besides, wind can also benefit for urban heat flows and then cool the land surface, but it could be blocked by tall or dense buildings. Therefore, it could also be beneficial for SUHI mitigation to improve the urban ventilation situation by increasing the standard deviation of building height and reducing the frontal area of buildings (Wang et al., 2021b). Furthermore, atmospheric circulation could also influence temperature, resulting in variations of SUHI intensities (Pórolnyczak et al., 2017); in particular, the intra-urban temperature differences are affected by atmospheric stability, which could amplify the differences of SUHI intensities among 3D neighborhoods (Krueger and Emmanuel, 2013). To reduce the uncertainty of our results, it is of high importance to monitor future atmospheric circulation. Besides, building shadows have some influences on estimating LST in areas with tall buildings; additionally, the dataset (such as land use map and population) used in our research were not all collected at the same time. Due to limited data sources, the above differences also contribute to some uncertainties in this study. As a result, we can use air temperature to evaluate the heat conditions of 3D neighborhoods in the future study; besides, future more detailed data could be used to comprehensively analyze SUHI intensities among 3D neighborhoods.

5. Conclusions

In spite of some uncertainties and limitations, this study is an important contribution to investigate urban 3D neighborhoods and their associated surface urban heat island (SUHI) intensities. Considering building height (BH) and building density (BSF), nine categories of urban 3D neighborhoods existed in 57 Chinese cities and HDMR (High Density & Medium Rise) contributed the largest share in China, followed by HDLR (High Density & Low Rise). However, the distribution of 3D neighborhoods varied among cities due to their distinct urban development levels, traditional cultures and natural geophysical conditions. The average SUHI intensity of all 3D neighborhoods can amount to 4.27 °C in China, with eastern and southern Chinese cities presenting higher SUHI intensities. However, Urumqi presented cold island effects since it was surrounded by desert. Considering 3D landscapes, SUHI intensities varied with different urban 3D neighborhoods, and the 3D neighborhoods of HDLR and HDMR presented higher SUHI intensities in most cities. The urban form indicator of the urban green index (UGI) had the largest relative contributions to SUHI intensities, followed by BH; these two dominant indicators can lead

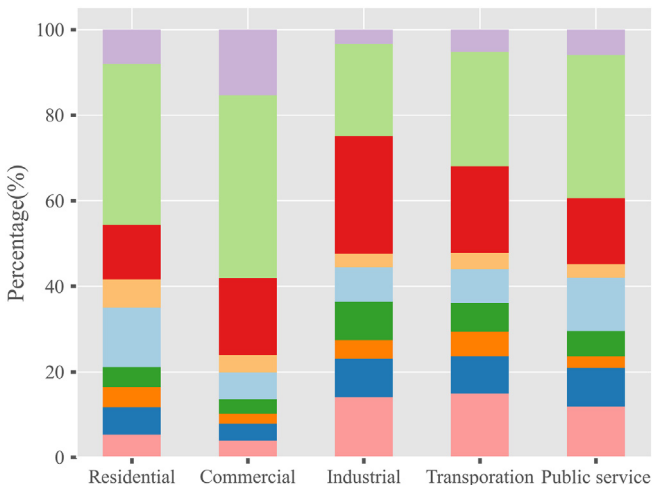


Fig. 9. 3D neighborhoods in different urban function zones.

to a total SUHI intensity change of 2.73 °C. The relative contributions of UGI decreased with the increase of building density and building height, but BH presented the opposite trend. The interaction of 3D landscape and function zones complicated urban thermal environments, with higher SUHI intensities in the industrial zone even among the same 3D neighborhoods. Besides, the SUHI intensities of 3D neighborhoods presented great diurnal and seasonal variations, with higher SUHI intensities in HDHR and HDMR at nighttime in winter and summer. What's more, urban residents may suffer unequal heat risk inside cities due to the deviations of SUHI intensities among different 3D neighborhoods. Therefore, it could be a highly effective way to mitigate SUHI effects in cities by increasing urban greening and improving urban ventilation.

CRediT authorship contribution statement

Yi Zhou: Conceptualization, Methodology, Software, Validation, Visualization, Writing-Original draft preparation. **Haile Zhao:** Investigation, Validation. **Sicheng Mao:** Methodology, Software. **Guoliang Zhang:** Investigation, Validation. **Yuling Jin:** Investigation, Validation. **Yuchao Luo:** Validation. **Wei Huo:** Validation. **Zhihua Pan:** Resources, Supervision, Funding acquisition. **Pingli An:** Resources, Supervision. **Fei Lun:** Conceptualization, Supervision, Writing - Review & Editing.

Data availability

Data will be made available on request.

Declaration of competing interest

The authors declare that they have no known competing financial interests or personal relationships that could have appeared to influence the work reported in this paper.

Acknowledgements

This work was supported by the National Key Research and Development Plan of China [2018YFA0606300].

Appendix A. Supplementary data

Supplementary data to this article can be found online at <https://doi.org/10.1016/j.scitotenv.2022.157662>.

References

- Amani-Beni, M., Zhang, B., Xie, G.-d., Xu, J., 2018. Impact of urban park's tree, grass and waterbody on microclimate in hot summer days: a case study of Olympic Park in Beijing, China. *Urban For. Urban Green.* 32, 1–6.
- Aram, F., García, E.H., Solgi, E., Mansournia, S., 2019. Urban green space cooling effect in cities. *Heliyon* 5, e01339.
- Bechtel, B., Demuzere, M., Mills, G., Zhan, W., Sismanidis, P., Small, C., et al., 2019. SUHI analysis using local climate zones—a comparison of 50 cities. *Urban Clim.* 28.
- Buyantuyev, A., Wu, J., 2010. Urban heat islands and landscape heterogeneity: linking spatio-temporal variations in surface temperatures to land-cover and socioeconomic patterns. *Landscape Ecol.* 25, 17–33.
- Cao, C., Li, X.-H., Zhang, M., Liu, S.-D., Xu, J.-P., 2017. Correlation analysis of the urban heat island effect and its impact factors in China. *Huan Jing Ke Xue* 38, 3987–3997.
- Chakraborty, T., Lee, X., 2019. A simplified urban-extent algorithm to characterize surface urban heat islands on a global scale and examine vegetation control on their spatiotemporal variability. *Int. J. Appl. Earth Obs. Geoinf.* 74, 269–280.
- Chakraborty, T., Hsu, A., Manya, D., Sheriff, G., 2019. Disproportionately higher exposure to urban heat in lower-income neighborhoods: a multi-city perspective. *Environ. Res. Lett.* 14, 105003.
- Changnon, S.A., 1992. Inadvertent weather modification in urban areas: lessons for global climate change. *Bull. Am. Meteorol. Soc.* 73, 619–627.
- Chen, B., Xu, B., Zhu, Z., Yuan, C., Suen, H.P., Guo, J., et al., 2019. Stable classification with limited sample: transferring a 30-m resolution sample set collected in 2015 to mapping 10-m resolution global land cover in 2017. *Sci. Bull.* 64, 370–373.
- Chen, B., Xie, M., Feng, Q., Li, Z., Chu, L., Liu, Q., 2021. Heat risk of residents in different types of communities from urban heat-exposed areas. *Sci. Total Environ.* 768, 145052.
- Cheng, W., Li, D., Liu, Z., Brown, R.D., 2021. Approaches for identifying heat-vulnerable populations and locations: a systematic review. *Sci. Total Environ.* 799, 149417.
- Cui, F., Hamdi, R., Yuan, X., He, H., Yang, T., Kuang, W., et al., 2021. Quantifying the response of surface urban heat island to urban greening in global north megacities. *Sci. Total Environ.* 801, 149553.
- Derdouri, A., Wang, R., Murayama, Y., Osaragi, T., 2021. Understanding the links between LULC changes and SUHI in cities: insights from two-decadal studies (2001–2020). *Remote Sens.* 13, 3654.
- Du, H., Wang, D., Wang, Y., Zhao, X., Qin, F., Jiang, H., et al., 2016. Influences of land cover types, meteorological conditions, anthropogenic heat and urban area on surface urban heat island in the Yangtze River Delta urban agglomeration. *Sci. Total Environ.* 571, 461–470.
- Estrada, F., Botzen, W.J.W., Tol, R.S.J., 2017. A global economic assessment of city policies to reduce climate change impacts. *Nat. Clim. Chang.* 7, 403–406.
- Fleming, L.E., Leonardi, G.S., White, M.P., et al., 2018. Beyond climate change and health: integrating broader environmental change and natural environments for public health protection and promotion in the UK[J]. *Atmosphere* 9 (7), 245.
- Garang, Z., Wu, C., Li, G., Zhuo, Y., Xu, Z., 2021. Spatio-temporal non-stationarity and its influencing factors of commercial land price: a case study of Hangzhou, China. *Land* 10, 317.
- Geletič, J., Lehnert, M., Savić, S., Milošević, D., 2019. Inter-/intra-zonal seasonal variability of the surface urban heat island based on local climate zones in three central European cities. *Build. Environ.* 156, 21–32.
- Gong, P., Chen, B., Li, X., Liu, H., Wang, J., Bai, Y., et al., 2020. Mapping essential urban land use categories in China (EULUC-China): preliminary results for 2018. *Sci. Bull.* 65, 182–187.
- Guo, H., Shi, Q., Marinoni, A., Du, B., Zhang, L., 2021. Deep building footprint update network: a semi-supervised method for updating existing building footprint from bi-temporal remote sensing images. *Remote Sens. Environ.* 264.
- Hamada, S., Ohta, T., 2010. Seasonal variations in the cooling effect of urban green areas on surrounding urban areas. *Urban For. Urban Green.* 9, 15–24.
- He, K., Huo, H., Zhang, Q., 2002. Urban air pollution in China: current status, characteristics, and progress. *Annu. Rev. Environ. Resour.* 27, 397.
- He, B.-J., Ding, L., Prasad, D., 2020. Relationships among local-scale urban morphology, urban ventilation, urban heat island and outdoor thermal comfort under sea breeze influence. *Sustain. Cities Soc.* 60.
- Heilmayer, O., Brey, T., 2003. Scaling of Metabolic Rate With Body Mass and Temperature in Scallops.
- Hong, J.W., Hong, J., Kwon, E.E., et al., 2019. Temporal dynamics of urban heat island correlated with the socio-economic development over the past half-century in Seoul, Korea[J]. *Environ. Pollut.* 254, 112934.
- Hu, L., Brunsell, N.A., 2013. The impact of temporal aggregation of land surface temperature data for surface urban heat island (SUHI) monitoring. *Remote Sens. Environ.* 134, 162–174.
- Huang, X., Wang, Y., 2019. Investigating the effects of 3D urban morphology on the surface urban heat island effect in urban functional zones by using high-resolution remote sensing data: a case study of Wuhan, Central China. *ISPRS J. Photogramm. Remote Sens.* 152, 119–131.
- Kedem, D., Tyree, S., Sha, F., Lanckriet, G.R., Weinberger, K.Q., 2012. Non-linear metric learning: Advances in neural information processing systems. Citeseer 2582–2590.
- Kim, S.W., Brown, R.D., 2021. Urban heat island (UHI) variations within a city boundary: a systematic literature review. *Renew. Sust. Energ. Rev.* 148.
- Krueger, E., Emmanuel, R., 2013. Accounting for atmospheric stability conditions in urban heat island studies: the case of Glasgow, UK. *Landsc. Urban Plan.* 117, 112–121.
- Kumar, R., Kaushik, S., 2005. Performance evaluation of green roof and shading for thermal protection of buildings. *Build. Environ.* 40, 1505–1511.
- Leconte, F., Bouyer, J., Claverie, R., Pétrissans, M., 2015. Using local climate zone scheme for UHI assessment: evaluation of the method using mobile measurements. *Build. Environ.* 83, 39–49.
- Li, S., Jiang, G.-M., 2018. Land surface temperature retrieval from Landsat-8 data with the generalized split-window algorithm. *IEEE Access* 6, 18149–18162.
- Li, W., Bai, Y., Chen, Q., He, K., Ji, X., Han, C., 2014. Discrepant impacts of land use and land cover on urban heat islands: a case study of Shanghai, China. *Econ. Indic.* 47, 171–178.
- Li, X., Zhou, Y., Gong, P., Seto, K.C., Clinton, N., 2020. Developing a method to estimate building height from Sentinel-1 data. *Remote Sens. Environ.* 240, 111705.
- Li, H., Li, Y., Wang, T., Wang, Z., Gao, M., Shen, H., 2021. Quantifying 3D building form effects on urban land surface temperature and modeling seasonal correlation patterns. *Build. Environ.* 204.
- Liang, Z., Wang, Y., Huang, J., et al., 2020. Seasonal and diurnal variations in the relationships between urban form and the urban heat island effect[J]. *Energies* 13 (22), 5909.
- Lin, P., Lau, S.S.Y., Qin, H., Gou, Z., 2017. Effects of urban planning indicators on urban heat island: a case study of pocket parks in high-rise high-density environment. *Landsc. Urban Plan.* 168, 48–60.
- Liu, J., Niyogi, D., 2020. Identification of linkages between urban heat island magnitude and urban rainfall modification by use of causal discovery algorithms. *Urban Clim.* 33.
- Logan, T., Zaitchik, B., Guikema, S., Nisbet, A., 2020. Night and day: the influence and relative importance of urban characteristics on remotely sensed land surface temperature. *Remote Sens. Environ.* 247, 111861.
- Long, Y., Li, P., Hou, J., 2019. Three-dimensional urban form at the street block level for major cities in China. *Shanghai Urban Plan. Rev.* 3, 10–15.
- Macintyre, H.L., Heaviside, C., Cai, X., Phalkey, R., 2021. The winter urban heat island: impacts on cold-related mortality in a highly urbanized European region for present and future climate. *Environ. Int.* 154, 106530.
- Mao, S., Zhou, Y., Gao, W., Jin, Y., Zhao, H., Luo, Y., et al., 2022. Ventilation capacities of Chinese industrial cities and their influence on the concentration of NO₂. *Remote Sens.* 14.
- Martin-Vide, J., Sarricolea, P., Moreno-García, M.C., 2015. On the definition of urban heat island intensity: the “rural” reference. *Front. Earth Sci.* 3, 24.

- Mashhoodi, B., 2021. Feminization of surface temperature: environmental justice and gender inequality among socioeconomic groups. *Urban Clim.* 40.
- Matsumoto, Ki, 2019. Climate change impacts on socioeconomic activities through labor productivity changes considering interactions between socioeconomic and climate systems. *J. Clean. Prod.* 216, 528–541.
- Merchant, C., Le Borgne, P., Marsouin, A., Roquet, H., 2008. Optimal estimation of sea surface temperature from split-window observations. *Remote Sens. Environ.* 112, 2469–2484.
- Mirzaei, P.A., 2015. Recent challenges in modeling of urban heat island. *Sustain. Cities Soc.* 19, 200–206.
- Motieyan, H., Azmoodeh, M., 2021. Mixed-use distribution index: a novel bilevel measure to address urban land-use mix pattern (A case study in Tehran, Iran). *Land Use Policy* 109.
- National Bureau of Statistics of China, 2021. 2021 China Urban Statistical Yearbook.
- Park, Y., Guldmann, J.-M., Liu, D., 2021. Impacts of tree and building shades on the urban heat island: combining remote sensing, 3D digital city and spatial regression approaches. *Comput. Environ. Urban. Syst.* 88, 101655.
- Pedregosa, F., Varoquaux, G., Gramfort, A., Michel, V., Thirion, B., Grisel, O., et al., 2011. Scikit-learn: machine learning in Python. *J. Mach. Learn. Res.* 12, 2825–2830.
- Peng, S., Piao, S., Ciais, P., Friedlingstein, P., Ottle, C., Fo-M, Bréon, et al., 2012. Surface urban heat island across 419 global big cities. *Environ. Sci. Technol.* 46, 696–703.
- Peng, J., Xie, P., Liu, Y., Ma, J., 2016. Urban thermal environment dynamics and associated landscape pattern factors: a case study in the Beijing metropolitan region. *Remote Sens. Environ.* 173, 145–155.
- Peng, J., Dan, Y., Qiao, R., Liu, Y., Dong, J., Wu, J., 2021. How to quantify the cooling effect of urban parks? Linking maximum and accumulation perspectives. *Remote Sens. Environ.* 252.
- Półtoraniczak, M., Kolendowicz, L., Majkowska, A., Czernecki, B., 2017. The influence of atmospheric circulation on the intensity of urban heat island and urban cold island in Poznań, Poland. *Theor. Appl. Climatol.* 127, 611–625.
- Qi, F., Zhai, J.Z., Dang, G., 2016. Building height estimation using Google earth. *Energy Build.* 118, 123–132.
- Sang, J., Liu, H., Liu, H., Zhang, Z., 2000. Observational and numerical studies of wintertime urban boundary layer. *J. Wind Eng. Ind. Aerodyn.* 87, 243–258.
- Sanyal, J., Lu, X.X., 2004. Application of remote sensing in flood management with special reference to monsoon Asia: a review. *Nat. Hazards* 33, 283–301.
- Stewart, I.D., Oke, T.R., 2012. Local climate zones for urban temperature studies. *Bull. Am. Meteorol. Soc.* 93, 1879–1900.
- Sun, F., Liu, M., Wang, Y., Wang, H., Che, Y., 2020a. The effects of 3D architectural patterns on the urban surface temperature at a neighborhood scale: relative contributions and marginal effects. *J. Clean. Prod.* 258, 120706.
- Sun, F., Liu, M., Wang, Y., Wang, H., Che, Y., 2020b. The effects of 3D architectural patterns on the urban surface temperature at a neighborhood scale: relative contributions and marginal effects. *J. Clean. Prod.* 258.
- Sun, Y., Wang, S., Wang, Y., 2020c. Estimating local-scale urban heat island intensity using nighttime light satellite imageries. *Sustain. Cities Soc.* 57, 102125.
- Ulpiani, G., 2021. On the linkage between urban heat island and urban pollution island: three-decade literature review towards a conceptual framework. *Sci. Total Environ.* 751, 141727.
- Varquez, A.C., Kanda, M., 2018. Global urban climatology: a meta-analysis of air temperature trends (1960–2009). *Npj Clim. Atmos. Sci.* 1, 1–8.
- Voogt, J.A., Oke, T.R., 2003. Thermal remote sensing of urban climates. *Remote Sens. Environ.* 86, 370–384.
- Wan, Z., Dozier, J., 1996. A generalized split-window algorithm for retrieving land-surface temperature from space. *IEEE Trans. Geosci. Remote Sens.* 34, 892–905.
- Wan, Z., Hook, S., Hulley, G., 2021. MODIS/Terra Land Surface Temperature/Emissivity 8-Day L3 Global 1km SIN Grid V061. distributed by NASA EOSDIS Land Processes DAAC <https://doi.org/10.5067/MODIS/MOD11A2.061> Accessed 2021-07-07.
- Wang, D., Shi, Y., Chen, G., Zeng, L., Hang, J., Wang, Q., 2021a. Urban thermal environment and surface energy balance in 3D high-rise compact urban models: scaled outdoor experiments. *Build. Environ.* 205.
- Wang, P., Goggins, W.B., Shi, Y., Zhang, X., Ren, C., Ka-Lun, La.u.K., 2021b. Long-term association between urban air ventilation and mortality in Hong Kong. *Environ. Res.* 197, 111000.
- Wu, Y., Fan, P., You, H., 2018. Spatial evolution of producer service sectors and its influencing factors in cities: a case study of Hangzhou, China. *Sustainability* 10, 975.
- Yang, Q., Huang, X., Tang, Q., 2019. The footprint of urban heat island effect in 302 Chinese cities: temporal trends and associated factors. *Sci. Total Environ.* 655, 652–662.
- Yao, L., Xu, Y., Zhang, B., 2019. Effect of urban function and landscape structure on the urban heat island phenomenon in Beijing, China. *Landsc. Ecol. Eng.* 15, 379–390.
- Yu, B., 2021. Ecological effects of new-type urbanization in China. *Renew. Sust. Energ. Rev.* 135.
- Yu, Z., Jing, Y., Yang, G., Sun, R., 2021. A new urban functional zone-based climate zoning system for urban temperature study. *Remote Sens.* 13.
- Zander, K.K., Cadag, J.R., Escarcha, J., Garnett, S.T., 2018. Perceived heat stress increases with population density in urban Philippines. *Environ. Res. Lett.* 13.
- Zhang, K., Wang, R., Shen, C., Da, L., 2010. Temporal and spatial characteristics of the urban heat island during rapid urbanization in Shanghai, China. *Environ. Monit. Assess.* 169, 101–112.
- Zhang, Y., Murray, A.T., Turner, J., 2017. Optimizing green space locations to reduce daytime and nighttime urban heat island effects in Phoenix, Arizona. *Landsc. Urban Plan.* 165, 162–171.
- Zhang, Y., Middel, A., Turner, B., 2019a. Evaluating the effect of 3D urban form on neighborhood land surface temperature using Google street view and geographically weighted regression. *Landsc. Ecol.* 34, 681–697.
- Zhou, D., Zhao, S., Zhang, L., Sun, G., Liu, Y., 2015a. The footprint of urban heat island effect in China. *Sci. Rep.* 5, 1–11.
- Zhou, Y., Smith, S.J., Zhao, K., Imhoff, M., Thomson, A., Bond-Lamberty, B., et al., 2015b. A global map of urban extent from nightlights. *Environ. Res. Lett.* 10, 054011.
- Zhou, Y., Zhang, G., Jiang, L., Chen, X., Xie, T., Wei, Y., et al., 2021. Mapping local climate zones and their associated heat risk issues in Beijing: based on open data. *Sustain. Cities Soc.* 74.
- Zhu, X.X., Qiu, C., Hu, J., Shi, Y., Wang, Y., Schmitt, M., et al., 2022. The urban morphology on our planet—Global perspectives from space. *Remote Sens. Environ.* 269, 112794.